Soft Matter

PAPER

View Article Online
View Journal | View Issue

Cite this: *Soft Matter*, 2018, **14**, 7214

Sweet surfactants: packing parameter-invariant amphiphiles as emulsifiers and capping agents for morphology control of inorganic particles†

Michael Voggel, Rebecca M. Meinusch, Vanessa Siewert, Marius Kunkel, Valentin Wittmann * and Sebastian Polarz *

Received 27th May 2018,
Accepted 13th July 2018

DOI: 10.1039/c8sm01091a

rsc.li/soft-matter-journal

Surfactants are not only pivotal constituents in any biological organism in the form of phospholipids, they are also essential for numerous applications benefiting from a large, internal surface, such as in detergents, for emulsification purposes, phase transfer catalysis or even nanoparticle stabilization. A particularly interesting, green class of surfactants contains glycoside head groups. Considering the variability of glycosides, a large number of surfactant isomers become accessible. According to established models in surfactant science such as the packing parameter or the hydrophilic lipophilic balance (HLB), they do not differ from each other and should, thus, have similar properties. Here, we present the preparation of a systematic set of glycoside surfactants and in particular isomers. We investigate to which extent they differ in several key features such as critical aggregation concentration, thermodynamic parameters, *etc.* Analytical methods like isothermal titration calorimetry (ITC), tensiometry, dynamic light scattering (DLS), small angle-X-ray scattering (SAXS), transmission electron microscopy (TEM) and others were applied. It was found that glycosurfactant isomers vary in their emulsification properties by up to two orders of magnitude. Finally, we have investigated the role of the surfactants in a microemulsion-based technique for the generation of zinc oxide (ZnO) nanoparticles. We found that the choice of the carbohydrate head has a marked effect on the shape of the formed inorganic nanocrystals.

1 Introduction

The generic term 'amphiphile' refers to substances, which are compatible with media characterized by different polarity. Regarding their polarity, solvents are typically considered either hydrophilic (water, alcohols) or hydrophobic (oils). Because of their unique property, amphiphiles are used in numerous applications involving media of different polarity, for example as detergents, emulsifiers, phase-transfer agents or as stabilizing agents in nanoparticle synthesis. Their ability to undergo self-assembly is another fascinating feature of amphiphiles. Classical examples are the formation of micelles or liquid crystalline phases.

Surfactants are one subclass among amphiphiles. They possess a well-defined molecular architecture, in which a hydrophilic head group is attached to a hydrophobic moiety, in most cases an alkyl chain. Surfactants can be further categorized according to their head group to be either ionic or non-ionic.[1] While the number of cationic or anionic groups is relatively limited, a large variety of non-ionic head groups exists, and their choice profoundly affects the properties of the surfactant.[2,3] Numerous non-ionic surfactants contain ethoxylates and oligo-ethylene glycol derivatives, respectively.

Surfactants with hydrophilic head groups cannot only be generated by *de novo* synthesis, they can also originate from the natural pool of organic compounds. For example, alkyl (poly)-glycosides are surfactants produced at a large scale (>300 000 t/a) from sustainable resources, such as starch and fat.[4] The obtained mixture of substances can vary in the number of carbohydrates, their anomeric configuration, and the degree of alkylation.[5] The chemistry of these carbohydrate surfactants was already established by E. Fischer in 1911,[6] and a comprehensive overview was given by Rybinski and Hill in 1998.[7] The advantages of carbohydrate surfactants are manifold and include biodegradability, chirality and low toxicity. Due to these properties, they find numerous applications in detergents and cosmetics. In more specialized applications they have been successfully used for the extraction and crystallization of proteins or for transfection.[8] Carbohydrate surfactants can also undergo self-assembly and form so-called niosomes, the synthetic analogues of liposomes.[9] Due to their enhanced stability, niosomes have

University of Konstanz, Department of Chemistry, Universitätsstraße 10, 78457 Konstanz, Germany. E-mail: valentin.wittmann@uni-konstanz.de, sebastian.polarz@uni-konstanz.de

† Electronic supplementary information (ESI) available: Additional information on synthetic procedures and molecular characterization data; additional data on surfactant self-assembly Fig. ESI-1–4. See DOI: 10.1039/c8sm01091a

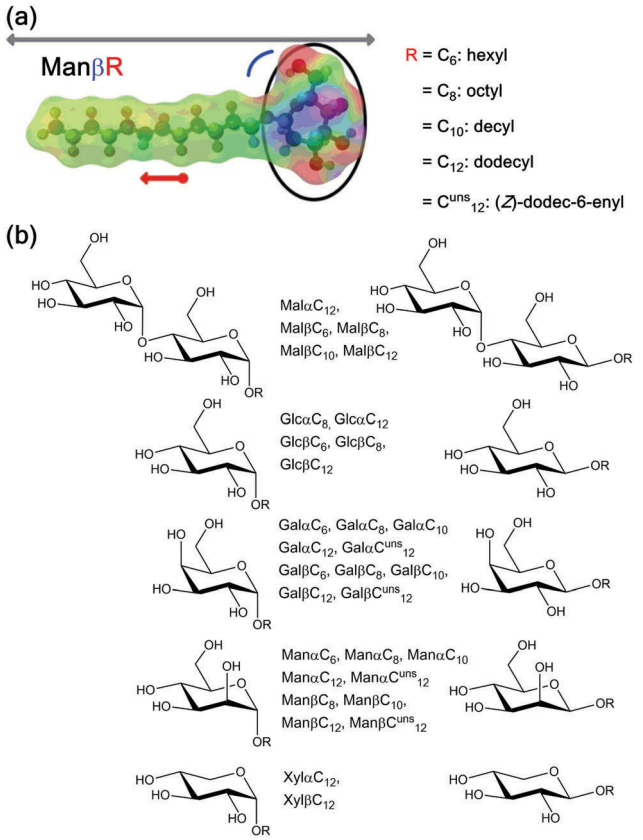

Fig. 1 (a) Possibilities for the generation of a systematic map of surfactants with carbohydrate head groups exemplarily shown for **ManβR**. Black = variation of carbohydrate head group; red = variation of the hydrophobic chain length (arrow); grey arrow = different surfactant length; blue = different anomeric configuration. Electrostatic potential map of a mannoside surfactant is also shown. (b) Overview of the surfactant library used in this study. Gal = galactose; Glc = glucose; Mal = maltose; Man = mannose, Xyl = xylose.

been successfully tested as biocompatible drug-delivery systems.[10] The application of glycoside surfactants in enantioselective phase transfer catalysis is highly interesting, but is still less explored.[11,12]

Further, carbohydrate-based surfactants are highly interesting from a fundamental perspective. The huge number of different carbohydrates and in particular the accessibility of various isomers makes sugar-based amphiphiles special.[13] In contrast to other systems, one can apply subtle differences to the structure of the surfactant head group region while maintaining key surfactant parameters such as the packing parameter or the HLB value (see also Fig. 1).

The packing parameter P is a widely used concept, which was introduced by Israelachvili.[14] P describes the shape of a surfactant taking into account the volume of the hydrophobic chain (V_0), the equilibrium area per molecule at the interface (A_{min}), and the length of the hydrophobic chain (l_0); $P = V_0/(A_{min} \cdot l_0)$. Another concept, which is particularly useful for classifying non-ionic surfactants, is the hydrophilic–lipophilic balance (HLB) introduced by Griffin.[15] The HLB value is proportional to the ratio of the molar mass of the hydrophilic moieties (M_h) of the surfactant and its total molecular mass (M); HLB = $20 \cdot (M_h/M)$. The HLB value can serve as first evidence, whether the surfactant might be appropriate for certain applications *e.g.* as oil-in-water emulsifier. A change of the surfactant structure normally results in a significant change of the packing and HLB parameters. Therefore, carbohydrate surfactants are ideal models for investigating, how even small changes in the surfactant structure can affect amphiphilic properties. Important work in this research field was done by Vill and coworkers.[16–18] Their studies mainly focused on the determination of the thermotropic behavior (clearing points)[16] and lyotropic phase diagrams obtained from polarization microscopy.[17,18] In 2014, Lindhorst and coworkers investigated the micellization behavior of a series of octyl glycoside surfactants by applying isothermal titration calorimetry (ITC) and diffusion ordered NMR spectroscopy.[19] They could show that the critical micelle concentration (CMC) value is influenced by the choice of carbohydrate and anomeric configuration.

Here, we present the investigation of a comprehensive, multidimensional library of glycoside surfactants (Fig. 1). In a systematic way, we studied the effect of different parameters, such as the nature of the tail and the head group. We investigated the effect of subtle variations of the head group including isomeric (glucose, galactose, mannose) or similar carbohydrates (xylose) as well as different anomeric configurations. Major effort has been put into the synthesis and isolation of surfactants in pure form. After thorough investigation of self-aggregation processes, we tested the use of the surfactants as emulsifiers. In a proof-of-concept experiment, we show that sugar-based surfactants can also function as capping agents influencing the morphology of inorganic zinc oxide nanoparticles grown in an emulsion-based method. This method was developed by us in the past,[20–23] however, glycoside surfactants had not yet been used as emulsifiers.

2 Experimental

2.1 General methods

N-Iodosuccinimide was purchased from abcr; Span 20 and Triton X-100 were purchased from TCI chemicals; octyl α-D-glucopyranoside (**GlcαC$_8$**), hexyl and octyl β-D-glucopyranoside (**GlcβC$_6$**, **GlcβC$_8$**), and hexyl β-D-maltoside (**MalβC$_6$**) were purchased from Sigma Aldrich; octyl, decyl, and dodecyl β-D-maltoside (**MalβC$_8$**, **MalβC$_{10}$**, **MalβC$_{12}$**) and dodecyl α-D-maltoside (**MalαC$_{12}$**) were purchased from Carbosynth. Isopropyl β-D-1-thiogalactoside (IPTG) was purchased from Carbolution Chemicals. All solvents were distilled prior to use and if required, dried according to standard procedures. All reactions were monitored by TLC on silica gel 60 F254 (Merck) on aluminum sheets with detection by UV-light (λ = 254 nm). Additionally, a solution of $Ce(SO_4)_2 \cdot 4H_2O$ (25 mM) and $(NH_4)_6Mo_7O_{24} \cdot 4H_2O$ (16 mM) in H_2SO_4 (10 wt%) followed by gentle heating was used for visualization. Preparative flash column chromatography (FC) was performed with silica 60 M (0.04–0.063 mm, Macherey-Nagel). NMR spectra were recorded at room temperature on Avance III 400 and Avance III 600 instruments from Bruker. Chemical shifts are reported in ppm relative to solvent signals ($CDCl_3$: δ_H = 7.26, δ_C = 77.16; DMSO-d_6: δ_H = 2.50, δ_C = 39.52). Signals were assigned by first order analysis and two-dimensional ^{1}H,^{1}H, ^{1}H,^{13}C and

^{1}H,^{31}P correlation spectroscopy (COSY, HSQC and HMBC). High-resolution electrospray ionization mass spectra (ESI-HRMS) were recorded on a Bruker micrOTOF II instrument.

2.2 Synthesis

2.2.1 General procedure for the synthesis of glycosurfactants by anomeric *O*-alkylation

(a) Formation of the triflated alcohol. A solution of alkyl alcohol (1.5 equiv.) and 2,6-lutidine (2.25 equiv.) in dry CH_2Cl_2 (15 mL g^{-1} alcohol) was cooled to 0 °C and triflic anhydride (2.1 equiv.) was added dropwise. After 15 min, *n*-hexane (30 mL g^{-1} alcohol) was added and the reaction mixture was washed with ice cold 0.1 M $KHSO_4$ solution, dried over Na_2SO_4 and concentrated under reduced pressure at 0 °C. The crude triflated alcohol was then immediately used without further purification.

(b) Anomeric O-alkylation[24]. A solution of the corresponding, previously prepared, 2,3,4,6-tetra-*O*-acetylhexose[25,26] (1 equiv.) in dry dimethoxyethane (10 mL g^{-1}) was cooled to 0 °C and sodium hydride (1.1 equiv., 60 wt% dispersion in mineral oil) was added portionwise. After gas evolution had ceased, the reaction mixture was cooled to −50 °C and the triflated alcohol, dissolved in dry dimethoxyethane (5 mL g^{-1} carbohydrate), was added and the reaction stirred overnight. The solvent was removed under reduced pressure and the remaining syrup was redissolved in ethyl acetate and washed with brine, dried over Na_2SO_4 and the solvent was evaporated. The crude product was purified by FC (petroleum ether/ethyl acetate) yielding the acetylated alkyl α- and β-D-*gluco*- and -mannopyranosides.

(c) Deprotection (Zemplén-protocol)[27]. The acetylated alkyl glucopyranoside or alkyl mannopyranoside was dissolved in dry MeOH (19 mL g^{-1}) and NaOMe (0.2 equiv., 0.5 M solution in MeOH) was added and stirred for 1 h. The reaction mixture was treated with Amberlite IR-120 ion exchange resin (H^+-form), filtered over celite and the solvent evaporated yielding the alkyl glucopyranoside or alkyl mannopyranoside (for details, yields, and product characterization see ESI†).

2.2.2 General procedure for the synthesis of glycosurfactants from IPTG. Isopropyl 2,3,4,5-tetra-*O*-benzyl-1-thio-β-D-galactopyranoside (**6**) was prepared from commercially available isopropyl 1-thio-β-D-galactopyranoside (IPTG) according to a procedure from Du *et al.*[28] To prepare the alkyl galactosides, a procedure from Ohlsson and Magnusson[29] was modified as follows. Benzylated thioglycoside (1 equiv.) and alkyl alcohol (1.1 equiv.) were dissolved in dry diethyl ether (50 mL g^{-1} thiogalactoside) and cooled to 0 °C (for high β-selectivity, the reaction is carried out in dry CH_2Cl_2 at −78 °C). NIS (1.2 equiv.) and TMSOTf (0.2 equiv.) were added. It was stirred for 1.5 h and NEt_3 (4.2 equiv.) was added. The reaction mixture was washed with $Na_2S_2O_3$ solution (10 wt%), saturated $NaHCO_3$ solution and water. The organic phase was dried over $MgSO_4$ and solvent evaporated. The crude product was purified and the anomers separated by FC (petroleum ether/ethyl acetate) yielding the benzylated alkyl α- and β-D-galactopyranosides. For deprotection, hydrogenation catalyst (10% palladium on carbon) was added to a solution of benzylated alkyl galactopyranoside in MeOH (22 mL $mmol^{-1}$). The mixture was vigorously stirred under a hydrogen atmosphere (1 atm) for two hours, filtered over celite, and the solvent was evaporated yielding the alkyl galactopyranosides (for details, yields, and product characterization see ESI†).

2.2.3 General procedure for the synthesis of saturated xylosides. To prepare the xylopyranosides, a procedure from Lopez and Fernandez-Mayoralas[30] was modified as follows. 1,2,3,4-Tetra-*O*-acetylxylose (1 equiv.) and alkyl alcohol (1.2 equiv.) were dissolved in dry CH_2Cl_2 (20 mL g^{-1}). $BF_3{\cdot}OEt_2$ (1 equiv.) was added dropwise and the mixture was stirred overnight. The reaction mixture was diluted with CH_2Cl_2, washed with saturated $NaHCO_3$ solution and water, and the organic phase was dried over $MgSO_4$ and the solvent evaporated. The crude product was purified and the anomers separated by FC (petroleum ether/ethyl acetate) yielding the acetylated alkyl α- and β-xylopyranosides. For deacetylation, the alkyl xylopyranosides were dissolved in dry MeOH (19 mL g^{-1}), NaOMe (0.5 M in MeOH, 0.15 equiv.) was added and the mixture stirred for 1 h. Then the mixture was neutralized with Amberlite IR-120 ion exchange resin (H^+-form), filtered over celite and the solvent evaporated yielding the alkyl xylopyranosides.

2.2.4 Synthesis of (*Z*)-dodec-6-en-1-ol[31] (3)

(6-Hydroxyhexyl)-triphenylphosphonium bromide. 6-Bromohexan-1-ol[32] (20.0 g, 110.4 mmol) was dissolved in dry acetonitrile (250 mL) and triphenylphosphine (30.4 g, 116 mmol) was added. The reaction mixture was heated to reflux for 24 h. Afterwards, the mixture was concentrated under reduced pressure and the residue redissolved in dry CH_2Cl_2, precipitated by addition of diethyl ether and freezing to −196 °C (to achieve full precipitation). After thawing, the supernatant was decanted. This procedure was repeated two times to ensure removal of excess triphenylphosphine. Remaining solvent was removed under reduced pressure to yield the phosphonium salt as white solid (43.9 g, 90%). ^{1}H NMR (400 MHz, $CDCl_3$): δ = 7.81–7.66 (m, 15 H, Ph), 3.68–3.61 (m, 2 H, H-1), 3.56 (t, J = 5.4 Hz, 2 H, H-6), 2.60 (s, 1 H, OH), 1.64 (s, 4 H, H-2, H-3), 1.49–1.42 (m, 4 H, H-4, H-5); ^{31}P NMR (162 MHz, $CDCl_3$): δ = 24.36 (s).

(Z)-Dodec-6-en-1-ol (3). NaH (60 wt% dispersion in mineral oil, 7.81 g, 195.5 mmol) was washed two times with dry *n*-hexane in order to remove the mineral oil. Then, dry DMSO (72 mL) was added and carefully heated to 75 °C until gas-evolution had ceased. The reaction mixture was diluted with dry THF (30 mL) and cooled to 0 °C. To the cooled mixture the phosphonium salt (43.3 g, 97.8 mmol), dissolved in dry DMSO (50 mL, 40 °C), was slowly added and stirred for 45 min. Subsequently, freshly distilled *n*-hexanal (12 mL, 97.7 mmol) was added dropwise and stirred for 20 min. Afterwards, the reaction mixture was poured on ice water and extracted with diethyl ether. After removal of the solvents, the residue was extracted with *n*-hexane. The combined extracts were washed with water, dried over $MgSO_4$ and the solvent evaporated. The crude product was purified *via* FC (petroleum ether/ethyl acetate 30 : 1) to yield 7.5 g (42%) of the alcohol (E : Z = 1 : 10) as colorless oil. R_f = 0.28 (petroleum ether/ethyl acetate 5 : 1); ^{1}H NMR of *Z*-product (400 MHz, $CDCl_3$): δ = 5.40–5.31 (m, 2 H, H-6, H-7), 3.63 (t, J = 6.6 Hz, 2 H, H-1), 2.06–1.96 (m, 4 H, H-5, H-8), 1.61–1.54 (m, 2 H, H-2) 1.39–1.24

(m, 10 H, H-4, H-9, H-3, H-11, H-10), 0.88 (t, J = 7.2 Hz, 3 H, H-12); ^{13}C NMR (101 MHz, $CDCl_3$): δ = 130.3 (C-6/7), 129.7 (C-6/7), 63.2 (C-1), 32.9 (C-2), 31.7 (C-10), 29.7 (C-9), 29.6 (C-4), 27.3 (C-5/8), 27.3 (C-5/8), 25.6 (C-3), 22.7 (C-11), 14.2 (C-12).

2.2.5 Synthesis of ManαC$^{uns}_{12}$ and ManβC$^{uns}_{12}$

*(Z)-Dodec-6-enyl 2,3,4,6-tetra-O-acetyl-α/β-D-mannopyranoside (**4α,4β**).* First, the triflated alcohol (21.82 mmol) was synthesized as described in 2.2.1. 2,3,4,6-Tetra-*O*-acetyl-D-mannopyranose (1, 5.06 g, 14.55 mmol) was dissolved in dry dimethoxyethane (80 mL) and cooled to 0 °C. NaH (60 wt% dispersion in mineral oil, 615 mg, 16 mmol) was added and after 10 min the triflated alcohol, dissolved in dimethoxyethane (20 mL), was added dropwise and the reaction stirred overnight. After removing solvent under reduced pressure, the residue was dissolved in ethyl acetate, washed with water and dried over Na_2SO_4. The solvent was evaporated and the crude product was purified by FC (petroleum ether/ethyl acetate = 10 : 1 to 6 : 1) to yield the pure α-product **4α** (3.26 g, 44%) and the β-product **4β** (500 mg, 7%) as slightly yellow solids. R_f(**4α**) = 0.49 (petroleum ether/ethyl acetate 3 : 1); R_f(**4β**) = 0.38 (petroleum ether/ethyl acetate 3 : 1); ^{1}H NMR of **4α** (400 MHz, $CDCl_3$): δ = 5.41–5.32 (m, 3 H, H-3, H-12, H-13), 5.27 (t, J = 10.0 Hz, 1 H, H-4), 5.23 (dd, J = 3.3 Hz, 2.5 Hz, 1 H, H-2), 4.80 (d, J = 1.3 Hz, 1 H, H-1), 4.28 (dd, J = 12.3 Hz, 5.4 Hz, 1 H, H-6a), 4.10 (dd, J = 12.2 Hz, 2.3 Hz, 1 H, H-6b), 3.98 (ddd, J = 12.3 Hz, 5.3 Hz, 2.3 Hz, 1 H, H-5), 3.67 (dt, J = 9.6 Hz, 6.9 Hz, 1 H, H-7a), 3.45 (dt, J = 9.6 Hz, 6.6 Hz, 1 H, H-7b), 2.15 (s, 3 H, Ac-2), 2.10 (s, 3 H, Ac-6), 2.04 (s, 3 H, Ac-4), 2.03 (m, 4 H, H-11, H-14), 1.99 (s, 3H, Ac-3), 1.61 (m, 2 H, H-8), 1.41–1.22 (m, 10 H, H-9, H-10, H-15, H-16, H-17), 0.89 (t, J = 6.8 Hz, 3 H, H-18); ^{13}C NMR of **4α** (101 MHz, $CDCl_3$): δ = 170.7 (Ac-6), 170.1 (Ac-2), 169.9 (Ac-3), 169.8 (Ac-4), 130.3 (C-12/13), 129.4 (C-12/13), 97.6 (C-1), 69.8 (C-2), 69.2 (C-3), 68.5 (C-5/7), 68.4 (C-5/7), 66.3 (C-4), 62.6 (C-6), 31.5 (C-16), 29.5 (C-9/10/15), 29.4 (C-9/10/15), 29.2 (C-8), 27.2 (C-11/14), 27.1 (C-11/14), 25.7 (C-9/10/15), 22.6 (C-17), 20.9 (C-Ac), 20.8 (C-Ac), 20.71 (C-Ac), 20.70 (C-Ac), 14.1 (C-18); ESI-HRMS: calcd for $C_{26}H_{42}O_{10}Na$ $[M + Na]^+$, 537.2669; found, 537.2762.

^{1}H NMR of **4β** (400 MHz, $CDCl_3$): δ = 5.47 (dd, J = 3.2 Hz, 0.8 Hz, 1 H, H-2), 5.34 (m, 2 H, H-12, H-13), 5.25 (t, J = 9.9 Hz, 1 H, H-4), 5.05 (dd, J = 9.9 Hz, 3.2 Hz, 1 H, H-3), 4.62 (d, J = 0.9 Hz, 1 H, H-1), 4.30 (dd, J = 12.2 Hz, 5.6 Hz, 1 H, H-6a), 4.15 (dd, J = 12.2 Hz, 4.2 Hz, 1 H, H-6b), 3.86 (dt, J = 9.4 Hz, 6.7 Hz, 1 H, H-7a), 3.66 (ddd, J = 9.9 Hz, 5.6 Hz, 4.2 Hz, 1 H, H-5), 3.49 (dt, J = 9.4 Hz, 6.9 Hz, 1 H, H-7b), 2.18 (s, 3 H, Ac-2), 2.09 (s, 3 H, Ac-6), 2.04 (s, 3 H, Ac-4), 2.01 (m, 4 H, H-11, H-14), 1.99 (s, 3 H, Ac-3), 1.59 (m, 2 H, H-8), 1.38–1.23 (m, 10 H, H-9, H-10, H-15, H-16, H-17), 0.88 (t, J = 6.8 Hz, 1 H, H-18); ^{13}C NMR of **4β** (101 MHz, $CDCl_3$): δ = 170.9 (Ac-6), 170.6 (Ac-2), 170.2 (Ac-3), 169.7 (Ac-4), 130.3 (C-12/13), 129.6 (C-12/13), 98.9 (C-1), 72.6 (C-5), 71.3 (C-3), 70.6 (C-7), 69.0 (C-2), 66.4 (C-4), 62.8 (C-6), 31.7 (C-16), 29.60 (C-9/10/15), 29.56 (C-9/10/15), 29.4 (C-8), 27.3 (C-11/14), 27.2 (C-11/14), 25.7 (C-9/10/15), 22.7 (C-17), 21.0 (C-Ac), 20.9 (C-Ac), 20.85 (C-Ac), 20.7 (C-Ac), 14.2 (C-18); ESI-HRMS: calcd for $C_{26}H_{42}O_{10}Na$ $[M + Na]^+$, 537.2669; found, 537.2672.

*(Z)-Dodec-6-enyl α-D-mannopyranoside (**ManαC$^{uns}_{12}$**).* (*Z*)-Dodec-6-enyl 2,3,4,6-tetra-*O*-acetyl-α-D-mannopyranoside (**4α**, 3.26 g, 6.34 mmol) was deprotected following the general procedure described in Section 2.2.1 to yield **ManαC$^{uns}_{12}$** as yellow solid (2.16 g, 98%). R_f = 0.41 (CH_2Cl_2/MeOH 5 : 1); ^{1}H NMR (400 MHz, DMSO-d_6): δ = 5.33 (m, 2 H, H-12, H-13), 4.67 (d, J = 5.3 Hz, 1 H, OH-4), 4.64 (d, J = 4.6 Hz, 1 H, OH-2), 4.57 (d, J = 1.4 Hz, 1 H, H-1), 4.50 (d, J = 5.9 Hz, 1 H, OH-3), 4.39 (d, J = 5.89 Hz, 1 H, OH-6), 3.67–3.60 (m, 1 H, H-6a), 3.60–3.54 (m, 2 H, H-2, H-7a), 3.47–3.40 (m, 2 H, H-3, H-6), 3.40–3.34 (m, 1 H, H-4), 3.30–3.24 (m, 2 H, H-5, H-7b), 2.07–1.88 (m, 4 H, H-11, H-14), 1.55–1.43 (m, 2 H, H-8), 1.38–1.19 (m, 10 H, H-9, H-10, H-15, H-16, H-17), 0.86 (t, J = 6.8 Hz, 3 H, H-18); ^{13}C NMR (101 MHz, DMSO-d_6): δ = 129.7 (C-12/13), 129.5 (C-12/13), 99.7 (C-1), 73.9 (C-5), 71.0 (C-3), 70.4 (C-2), 67.0 (C-4), 66.2 (C-7), 61.3 (C-6), 30.8 (C-16), 28.93 (C-9/10/15), 28.87 (C-9/10/15), 28.8 (C-8), 26.58 (C-11/14), 26.55 (C-11/14), 25.4 (C-9/10/15), 21.9 (C-17), 13.9 (C-18); ESI-HRMS: calcd for $C_{18}H_{34}O_6Na$ $[M + Na]^+$, 369.2246; found, 369.2208.

*(Z)-Dodec-6-enyl β-D-mannopyranoside (**ManβC$^{uns}_{12}$**).* (*Z*)-Dodec-6-enyl 2,3,4,6-tetra-*O*-acetyl-β-D-mannopyranoside (**4β**, 498 mg, 0.97 mmol) was deprotected following the general procedure described in Section 2.2.1 to yield **ManβC$^{uns}_{12}$** as yellow solid (322 mg, 96%). R_f = 0.43 (CH_2Cl_2/MeOH 5 : 1); ^{1}H NMR (400 MHz, DMSO-d_6): δ [ppm] = 5.39–5.29 (m, 2 H, H-12, H-13), 4.69 (d, J = 4.9 Hz, 1 H, OH-4), 4.49 (d, J = 5.9 Hz, 1 H, OH-3), 4.39 (t, J = 5.9 Hz, 1 H, OH-6), 4.33 (s, 1 H, H-1), 4.23 (d, J = 5.0 Hz, 1 H, OH-2), 3.75 (dt, J = 9.8 Hz, 7.2 Hz, 1 H, H-7a), 3.71–3.63 (m, 1 H, H-6a), 3.63–3.58 (m, 1 H, H-2), 3.48–3.36 (m, 2 H, H-6b, H7-b), 3.29–3.19 (m, 2 H, H-4, H-3), 3.04–2.97 (m, 1 H, H-5), 2.07–1.88 (m, 4 H, H-11, H-14), 1.56–1.45 (m, 2 H, H-8), 1.37–1.39 (m, 10 H, H-9, H-10, H-15, H-16, H-17), 0.86 (t, J = 6.8 Hz, 3 H, H-18); ^{13}C NMR (101 MHz, DMSO-d_6): δ = 129.7 (C-12/13), 129.6 (C-12/13), 100.2 (C-1), 77.5 (C-5), 73.7 (C-3), 70.6 (C-2), 68.3 (C-7), 67.2 (C-4), 61.4 (C-6), 30.8 (C-16), 29.1 (C-9/10/15), 29.0 (C-9/10/15), 28.8 (C-8), 26.61 (C-11/14), 26.56 (C-11/14), 25.2 (C-9/10/15) 21.9 (C-17), 13.9 (C-18); ESI-HRMS: calcd for $C_{18}H_{34}O_6Na$ $[M + Na]^+$, 369.2246; found, 369.2307.

2.2.6 Synthesis of GalαC$^{uns}_{12}$ and GalβC$^{uns}_{12}$

*(Z)-Dodec-6-enyl 2,3,4,6-tetra-O-acetyl-α/β-D-galactopyranoside (**5α,5β**).* First, the triflated alcohol (1.5 equiv.) was synthesized as described in Section 2.2.1. 2,3,4,6-Tetra-*O*-acetyl-D-galactopyranose (2, 1.26 g, 3.62 mmol) was dissolved in dry dimethoxyethane (20 mL) and cooled to −50 °C. NaH (60 wt% dispersion in mineral oil, 159.3 mg, 3.98 mmol) was added. After 10 min, the triflated alcohol, dissolved in dimethoxyethane (20 mL), was added dropwise and the reaction stirred overnight. After removing the solvent under reduced pressure, the residue was dissolved in ethyl acetate, washed with water and dried over Na_2SO_4. The solvent was evaporated and the crude product was purified by FC (petroleum ether/ethyl acetate = 10 : 1 to 6 : 1) to yield the pure α-product **5α** (244 mg, 13%) and the β-product **5β** (1.17 g, 63%) as white solids. R_f(**5α**) = 0.20 (petroleum ether/ethyl acetate 5 : 1); R_f(**5β**) = 0.14 (petroleum ether/ethyl acetate 5 : 1); ^{1}H NMR of **5α** (400 MHz, $CDCl_3$): δ = 5.46–5.45 (dd, J = 3.4 Hz, 1.2 Hz, 1 H, H-4), 5.40–5.30 (m, 3 H, H-2, H-12, H-13), 5.12–5.09 (m, 2 H, H-3, H-1), 4.22 (dt, J = 6.3 Hz, 1.2 Hz, 1 H, H-5), 4.09 (ddd, J = 6.3 Hz, 3.2 Hz, 2.3 Hz, 2 H, H-6), 3.68 (dt, J = 9.9 Hz, 6.5 Hz, 1 H,

H-7a), 3.42 (dt, J = 9.9 Hz, 6.5 Hz, 1 H, H-7b), 2.14 (s, 3 H, Ac-4), 2.07 (s, 3 H, Ac-3), 2.04 (s, 3 H, Ac-6), 2.02 (m, 4-H, H-11, H-14), 1.98 (s, 3 H, Ac-2), 1.61–1.57 (m, 2 H, H-8), 1.38–1.27 (m, 10 H, H-10, H-15, H-9, H-17, H-16), 0.88 (d, J = 13.2 Hz, 3 H, H-18); ^{13}C NMR of **5α** (101 MHz, $CDCl_3$): δ = 170.6 (Ac-3), 170.5 (Ac-6), 170.4 (Ac-4), 170.2 (Ac-2), 130.4 (C-12/13), 129.5 (C-12/13), 96.3 (C-1), 68.8 (C-7), 68.4 (C-3), 68.3 (C-4), 67.9 (C-2), 66.3 (C-5), 62.0 (C-6), 32.7 (C-16), 31.7 (C-9/10/15), 29.6 (C-9/10/15), 29.4 (C-8), 27.4 (C-11/14), 27.3 (C-11/14), 25.9 (C-9/10/15), 22.7 (C-17), 20.9 (Ac-3), 20.84 (Ac-6), 20.82 (Ac-4), 20.80 (Ac-2), 14.2 (C-18); ESI-HRMS: calcd for $C_{26}H_{42}O_{10}Na$ $[M + Na]^+$, 537.2669; found, 537.2742.

^{1}H NMR of **5β** (400 MHz, $CDCl_3$): δ = 5.38 (dd, J = 3.5 Hz, 1.0 Hz, 1 H, H-4), 5.36–5.29 (m, 2 H, H-12, H-13), 5.20 (dd, J = 10.5 Hz, 8.0 Hz, 1 H, H-2), 5.01 (dd, J = 10.5 Hz, 3.5 Hz, 1 H, H-3), 4.45 (d, J = 8.0 Hz, 1 H, H-1), 4.20–4.10 (m, 2 H, H-6), 3.91–3.85 (m, 2 H, H-5, H-7a), 3.46 (dt, J = 9.7 Hz, 7.0 Hz, 1 H, H-7b), 2.14 (s, 3 H, Ac-4), 2.04 (m, 6 H, Ac-2, Ac-6), 2.01 (m, 4 H, H-11, H-14), 1.98 (s, 3 H, Ac-3) 1.64–1.55 (m, 2 H, H-8), 1.35–1.25 (m, 10 H, H-9, H-10, H-15, H-16, H-17), 0.88 (t, J = 6.9 Hz, 3 H, H-18); ^{13}C NMR of **5β** (101 MHz, $CDCl_3$): δ = 170.5 (Ac-6), 170.4 (Ac-4), 170.3 (Ac-3), 169.5 (Ac-2), 130.4 (C-12/13), 129.6 (C-12/13), 101.5 (C-1), 71.1 (C-3), 70.7 (C-5), 70.3 (C-7), 69.1 (C-2), 67.2 (C-4), 61.4 (C-6), 31.7 (C-16), 29.6 (C-8), 29.55 (C-10), 29.48 (C-15), 27.3 (C-11/14), 27.3 (C-11/14), 25.6 (C-9), 22.7 (C-17), 21.2 (Ac-4), 20.9 (Ac-2), 20.8 (Ac-6), 20.7 (Ac-3), 14.2 (C-18); ESI-HRMS: calcd for $C_{26}H_{42}O_{10}Na$ $[M + Na]^+$, 537.2669; found, 537.2761.

*(Z)-Dodec-6-enyl α-D-galactopyranoside (**GalαC$^{uns}_{12}$**).* (*Z*)-Dodec-6-enyl 2,3,4,6-tetra-*O*-acetyl-α-D-galactopyranoside (**5α**, 234 mg, 0.455 mmol) was deprotected following the general procedure described in Section 2.2.1 to yield **GalαC$^{uns}_{12}$** as white solid (194 mg, 94%). R_f = 0.28 (CH_2Cl_2/MeOH 10 : 1); ^{1}H NMR (400 MHz, DMSO-d_6): δ = 5.39–5.29 (m, 2 H, H-12, H-13), 4.61 (d, J = 3.5 Hz, 1 H, H-1), 4.50–4.48 (m, 2 H, OH-6, OH-3), 4.35 (d, J = 6.3 Hz, 1 H, OH-2), 4.31 (d, J = 4.3 Hz, 1 H, OH-4), 3.69 (t, J = 3.1 Hz, 1 H, H-4), 3.59–3.47 (m, 5 H, H-7a, H-2, H-5, H-3, H-6a), 3.45–3.39 (m, 1 H, H-6b), 3.29–3.27 (m, 1 H, H-7b), 1.99–1.96 (m, 4 H, H-11, H-14), 1.53–1.50 (m, 2 H, H-8), 1.24–1.25 (m, 12 H, H-9, H-10, H-15, H-16, H-17), 0.86 (t, J = 6.7 Hz, 3 H, H-18); ^{13}C NMR (101 MHz, DMSO-d_6): δ = 129.7 (C-12/13), 129.6 (C-12/13), 98.8 (C-1), 71.1 (C-2/3/5), 69.6 (C-4), 68.9 (C-2/3/5), 68.4 (C-2/3/5), 66.8 (C-7), 60.6 (C-6), 30.8 (C-16/17), 29.0 (C-8), 28.8 (C-9/10/15), 26.6 (C-11/14), 26.55 (C-11/14), 25.4 (C-9/10/15), 21.9 (C-16/17), 13.9 (C-18); ESI-HRMS: calcd for $C_{18}H_{34}O_6Na$ $[M + Na]^+$, 369.2246; found, 369.2226.

*(Z)-Dodec-6-enyl β-D-galactopyranoside (**GalβC$^{uns}_{12}$**).* (*Z*)-Dodec-6-enyl 2,3,4,6-tetra-*O*-acetyl-β-D-galactopyranoside (**5β**, 1.17 g, 2.28 mmol) was deprotected following the general procedure described in Section 2.2.1 to yield **GalβC$^{uns}_{12}$** as white solid (831 mg, 92%). R_f = 0.53 (CH_2Cl_2/MeOH 5 : 1); ^{1}H NMR (400 MHz, DMSO-d_6): δ = 5.39–5.29 (m, 2 H, H-12, H-13), 4.75 (d, J = 4.0 Hz, 1 H, OH-2), 4.64 (s, 1 H, OH-3), 4.52 (t, J = 5.6 Hz, 1 H, OH-6), 4.30 (d, J = 4.5 Hz, 1 H, OH-4), 4.04 (d, J = 7.3 Hz, 1 H, H-1), 3.71 (dt, J = 9.6 Hz, 6.8 Hz, 1 H, H-7a), 3.62 (s, 1 H, H-4), 3.55–3.44 (m, 2 H, H-6), 3.39 (dt, J = 9.5 Hz, 6.7 Hz, 1 H, H-7b), 3.30–3.28 (m, 1 H, H-5), 3.26–3.24 (m, 2 H, H-2, H-3), 2.01–1.96 (m, 4 H, H-11, H-14), 1.53–1.50 (m, 2 H, H-8), 1.32–1.23 (m, 12 H, H-9, H-10, H-15, H-16, H-17), 0.86 (t, J = 6.6 Hz, 3 H, H-18); ^{13}C NMR (101 MHz, DMSO-d_6): δ = 129.64 (C-12/13), 129.56 (C-12/13), 103.5 (C-1), 75.1 (C-5), 73.5 (C-2/3), 70.5 (C-2/3), 68.4 (C-7), 68.1 (C-4), 60.4 (C-6), 30.8 (C-16/17), 29.2 (C-9/10/15), 29.0 (C-9/10/15), 28.8 (C-8), 26.6 (C-11/14), 26.55 (C-11/14), 25.2 (C-9/10/15), 21.9 (C-16/17), 13.9 (C-18); ESI-HRMS: calcd for $C_{18}H_{34}O_6Na$ $[M + Na]^+$, 369.2246; found, 369.2250.

2.2.7 General procedure for emulsion-based ZnO-particle synthesis. The hetero cubane precursor $[MeZno^iPr]_4$ was prepared according to a procedure by Lizandara-Pueyo.[20] 62.5 mg of the respective glycosurfactant were dissolved in 35 mL warm cyclohexane (40 °C), 1.5 mL water was added and an emulsion was prepared by applying ultrasound for 10 minutes using a Bandelin-Sonoplus HD3100-MS73. The emulsion was heated to 55 °C and a solution of 1 g $[MeZnO^iPr]_4$ in 10 mL dry cyclohexane was added at a rate of 0.55 mL min^{-1}. Ultrasound was applied during addition and for additional 8 h afterwards. The solvent was removed under reduced pressure to obtain ZnO nanoparticles as a white powder.

2.2.8 General procedure for emulsion experiments. For a typical experiment, a mixture of 6 mL cyclohexane, 6 mL water and 53.4 mg surfactant (0.5 wt%) was ultrasonicated for one min and the formed emulsion immediately transferred into a 10 mL measuring cylinder with a 14/23 ground glass joint (to prevent solvent evaporation). The volume of separated and emulsion phase was monitored over time.

2.2.9 Molecular structures and electrostatic potential mapping. Molecular structures were drawn in Avogadro and their geometry optimized using MMFF94 force field optimization. Electrostatic potential maps of the optimized structures were calculated in Maestro (Schrödinger).

2.3 Analytical techniques

2.3.1 Isothermal titration calorimetry (ITC). Isothermal titration calorimetry experiments were performed on a GE Microcal iTC$_{200}$ system at 20 °C. For a typical experiment (CAC < 100 mM), a solution with a concentration of approx. 10-fold CAC was prepared in milliQ-water. This solution was titrated into milliQ-water at 750 rpm stirring speed and with 120 s initial delay for equilibration. Depending on the amount of heat generated, the reference power was adjusted. Usually, 39 injections of 1 μL each were performed, with a 0.4 μL injection prior to the first injection. The data were processed using Origin 7 with the iTC Data analysis plugin, applying manual baseline correction and manual integration if necessary. The integrated data was transferred to Excel, correct concentration values were recalculated, plotted in Origin 2018 and fitted with a sigmoidal function. The free energy (ΔG°_{demic}), enthalpy (ΔH°_{demic}) and entropy (ΔS°) of the demicellation process were calculated based on the phase separation model using the following equations[19,33] (with molar fraction CAC′, observed reaction enthalpy $\Delta_R H^\circ$ and the concentration of injected surfactant solution $c_{syringe}$):

$$\Delta G^\circ_{demic} = -RT \ln \mathrm{CAC}' = \Delta H^\circ_{demic} - T\Delta S^\circ$$

$$\Delta H^\circ_{demic} = \Delta_R H^\circ_{demic} \cdot c_{syringe} / (c_{syringe} - \mathrm{CAC})$$

For determination of CAC > 100 mM, a diluted solution of the surfactant (approx. 0.5-fold CAC) was placed in the sample cell, in which and a concentrated surfactant solution (approx. 2.5–3-fold CAC) was titrated. Due to the smaller concentration window, multiple titration cycles were performed consecutively while removing the supernatant solution after each cycle. Each data set was processed as described before, plotted in Origin 2018, and the combined titrations were fitted with a sigmoidal function.

2.3.2 Dynamic light scattering (DLS). Dynamic light scattering measurements were conducted on a Malvern Zetasizer μV at 90° scattering angle. For each surfactant, a series of concentrations (5-, 4-, 3-, 2-, 1-, 0.5- and 0.1-fold CAC) was evaluated. All solutions were filtered using CHROMAFIL 0.45 μm PVDF syringe adapter filters.

2.3.3 Tensiometry. Surface tension γ measurements were performed on a Krüss K100 tensiometer at 20 °C with aqueous surfactant solutions with a concentration $c >$ CAC. For poorly soluble surfactants, saturated solutions were used. CACs were determined by the intersection point of linear regressions of the curves at $c >$ CAC and $c <$ CAC. The slope of the curve at $c <$ CAC ($\mathrm{d}\gamma/\mathrm{d}\log c$) was used to calculate the surface excess concentration $\Gamma_{\max}$ and the minimum molecular area occupied $A_{\min}$ by[34]

$$\Gamma_{\max} = -(2.303RT)^{-1}\cdot(\mathrm{d}\gamma/\mathrm{d}\log c)$$

$$A_{\min} = (N_A\cdot\Gamma_{\max})^{-1}$$

2.3.4 Small angle- and powder X-ray diffraction (SAXS/PXRD). SAXS diffractograms of surfactant samples were acquired on a Bruker Nanostar system equipped with pinhole collimation and $Cu_{K\alpha}$ radiation. All samples were equilibrated at air prior to measurements. PXRD-diffractograms of ZnO nanoparticles were recorded on a Bruker D8 system.

2.3.5 Polarization microscopy. Polarization microscopy images were acquired on an Olympus CX41 microscope with crossed polarization filters.

2.3.6 Transmission electron microscopy (TEM). TEM micrographs were acquired on a JEOL JEM-2200FS.

3 Results and discussion

3.1 Library of glycosurfactants

Fig. 1 gives an overview of the glycosurfactants used in our studies. We included compounds with mono-hexose-type head groups ranging from the well-known glucose surfactants over galactose and mannose to xylose derivatives. Compounds with the same length of the saturated hydrophobic side chain are either true isomers (for glucose, galactose, and mannose) or at least very similar (xylose differs from glucose only by a missing hydroxymethyl group). Therefore, these amphiphiles formally do not differ in their packing parameter *P* or HLB value. The same is true, if the anomeric configuration (α,β) is varied. A significant change in the head group region is realized for the surfactants containing the disaccharide maltose. A variation of the hydrocarbon chain length will obviously affect *P* and HLB. Beside surfactants with a saturated alkyl chain, we also included novel galactoside and mannoside surfactants with an unsaturated chain. This structural variation can also be regarded as almost *P* and HLB invariant.

3.2 Synthesis of glycosurfactants

Except for some glycosurfactants that were commercially available, the members of the library were synthesized either by anomeric *O*-alkylation (**Glcα/βC$_{12}$**, **Galα/βC$^{uns}_{12}$**, **Manα/βC$_n$**, **Manα/βC$^{uns}_{12}$**), by NIS-promoted glycosylation of thiogalactoside **6** (**Galα/βC$_n$**), or by Lewis-acid catalyzed glycosylation of peracetylated xylose **7** (**Xylα/βC$_{12}$**) as shown in Fig. 2. For the synthesis of **Galα/βC$^{uns}_{12}$** and **Manα/βC$^{uns}_{12}$** by anomeric *O*-alkylation, (*Z*)-dodec-6-en-1-ol (**3**) was triflated using triflic anhydride and then reacted with 2,3,4,6-tetra-*O*-acetylated mannose **1** or galactose **2** and sodium hydride to obtain the glycosides **4** and **5**, respectively, as mixtures of anomers (Fig. 2a). The anomers could be separated by flash chromatography to obtain **4α** (44%), **4β** (7%), **5α** (13%), and **5β** (63%). Subsequent deacetylation under Zémplen conditions gave the unsaturated glycosurfactants in high yields. Being stereoisomers, all four compounds lead to identical high-resolution mass spectra (Fig. 2b).

For the synthesis of the saturated galactosides, we reacted benzylated thiogalactoside **6**, which is conveniently obtained from commercially available IPTG in one step, with the respective alcohol in presence of NIS. After separation of the anomers by flash chromatography and debenzylation, pure glycosurfactants were obtained. For the synthesis of **Xylα/βC$_{12}$**, peracetylated xylose **7** was activated with BF_3 etherate and reacted with dodecanol. Interestingly, this reaction gave high amounts of the α-anomer despite the presence of the neighboring group-active acetyl group in the 2-position. Zémplen deacetylation gave the xylose surfactants.

All new compounds were fully characterized by ^{1}H and ^{13}C NMR spectroscopy as well as ESI-HRMS. The anomeric configuration was determined from the $^3J_{H\text{-}1,H\text{-}2}$ coupling constants for all glucosides, galactosides, and xylosides. For the mannosides, we relied on heteronuclear $^1J_{C\text{-}1,H\text{-}1}$ coupling constants that were obtained from non-decoupled ^{1}H,^{13}C HSQC spectra. Exemplarily, the values for **Manα/βC$^{uns}_{12}$** are 170 Hz (α-anomer) and 155 Hz (β-anomer) which is in agreement with reported values for mannosides.[35]

3.3 Surfactant properties

To get a first impression of similarities and differences between the surfactants, we generated optimized molecular structures with electrostatic potential mapping of the surfactants (*cf.* Fig. 1). It is obvious that the packing parameter and the HLB value are mainly influenced by two factors: the number of hexose units in the head group ($HLB_{\mathbf{Glc\beta C_{12}}}$ = 10.3 → $HLB_{\mathbf{Mal\beta C_{12}}}$ = 13.3) and the length of the hydrophobic chain ($HLB_{\mathbf{Glc\beta C_6}}$ = 13.6 → $HLB_{\mathbf{Glc\beta C_{10}}}$ = 11.2). Considering the situation for different isomers of the surfactants, the HLB value and also the packing parameter will remain similar. The incorporation of a double bond should also only slightly influence these parameters. Therefore, we expected the surfactants with maltose head groups

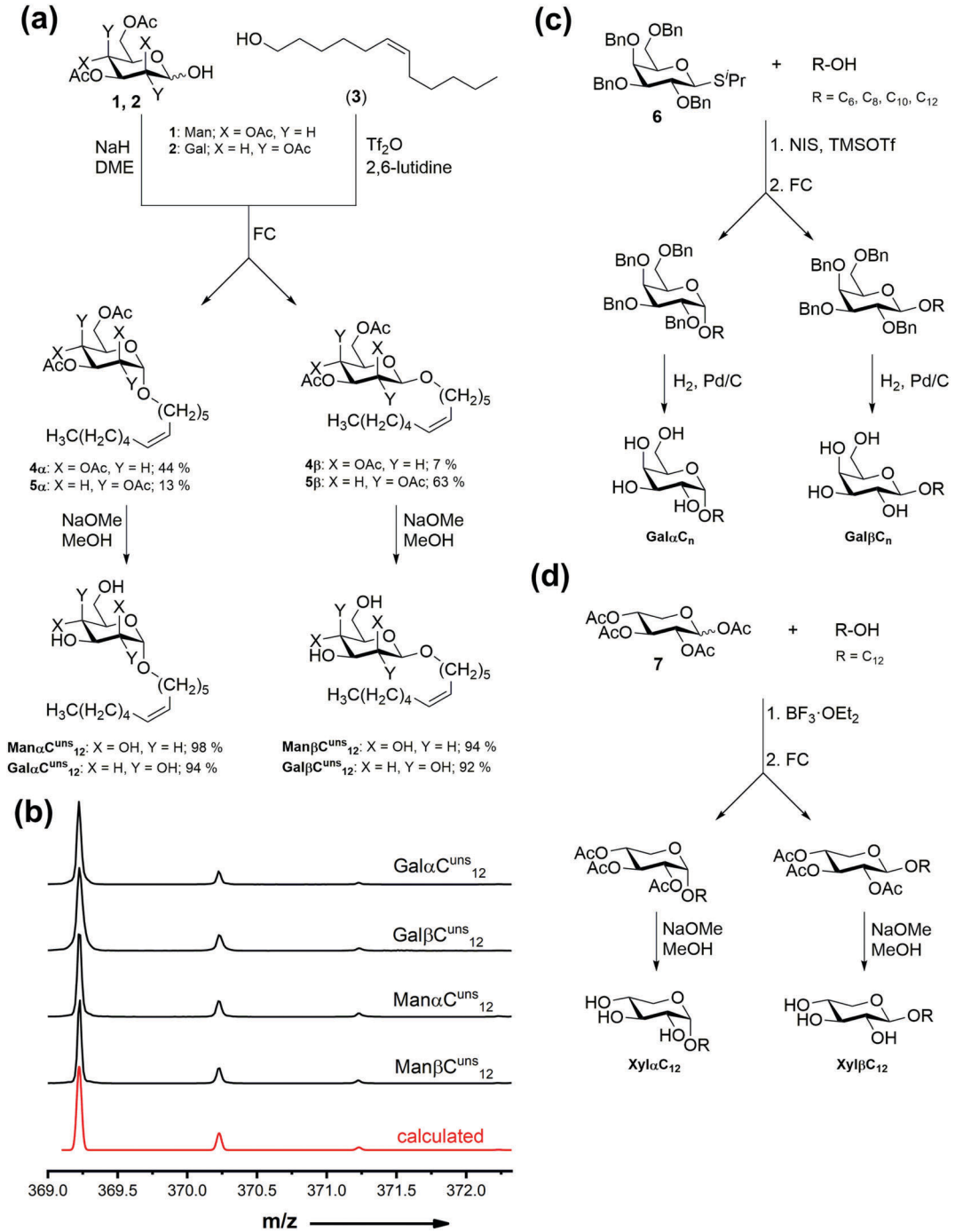

Fig. 2 (a) Synthesis of **Manα/βC$^{uns}_{12}$** and **Galα/βC$^{uns}_{12}$** by anomeric *O*-alkylation. (b) ESI-HRMS spectra of the newly synthesized carbohydrate surfactants with unsaturated side chain. Experimental (black) and calculated spectra (red) of the Na^+ adduct. (c) Synthesis of **Galα/βC$_n$** from thiogalactoside **6**. (d) Synthesis of **Xylα/βC$_{12}$**.

to behave differently than the monosaccharide derivatives, in agreement to literature.[36] It seems that the anomeric configuration also has a noticeable effect because at least for our calculations the molecular structures are different when comparing the α- and the β-form (for an example see Fig. 1a). The latter expectation is also in line with the literature.[19] To further study these hypotheses and findings, we systematically checked the key properties of the surfactants of our library.

3.3.1 Lyotropic liquid crystal formation. Surfactants form higher organized structures induced by a microphase separation of hydrophobic and hydrophilic domains. At higher concentration, one can observe the occurrence of lyotropic liquid crystal (LLC) phases in contact to water. Because many LLC phases are optically anisotropic, it is possible to use optical polarization microscopy (POLMIC) as a quick tool for checking for their presence. POLMIC images of selected examples are shown in Fig. 3a–c.

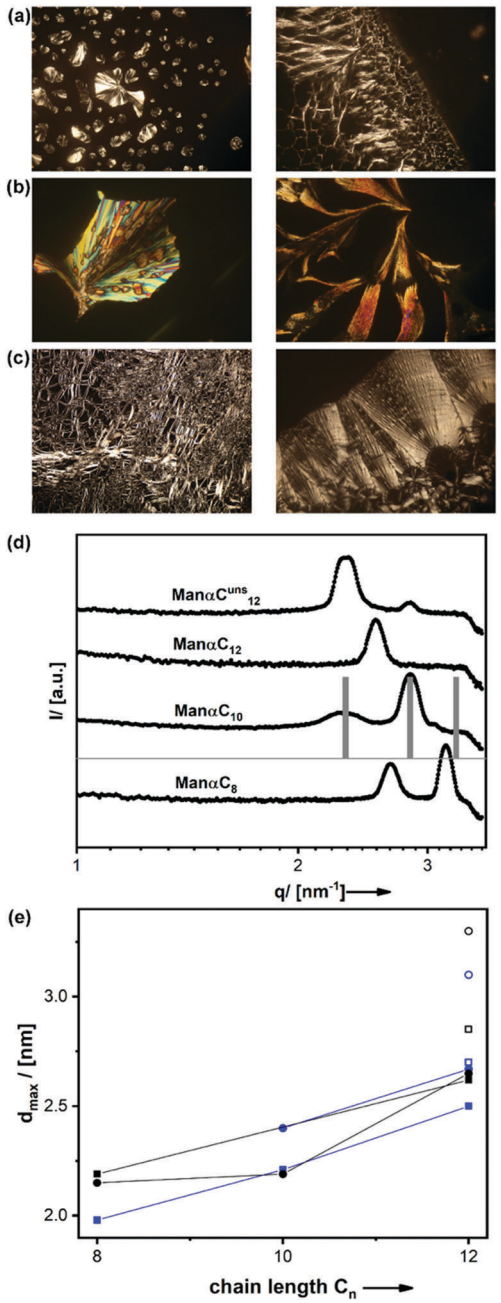

Fig. 3 POLMIC images of α- (left) and β-anomers (right) for **ManC$_{12}$** (a), **GalC$_{12}$** (b) and **GalC$^{uns}_{12}$** (c). (d) SAXS patterns of **ManαC$_8$**, **ManαC$_{10}$**, **ManαC$_{12}$** and **ManαC$^{uns}_{12}$**. The grey bars indicate the pattern expected for a OBDD phase with a periodicity of 3.8 nm. (e) d_{max}-dependence on chain length C_n of surfactant samples equilibrated at air. Gal (black), Man (blue), α (squares), β (circles), C_n (solid symbols), $C^{uns}{}_n$ (hollow symbols).

Although the assignment of a microstructure from POLMIC textures is often difficult, it becomes visible that the change of the head group Man→Gal (a,b), the anomeric configuration α→β (a,b,c), and also the shape of the tail C_{12}→$C^{uns}{}_{12}$ (b,c) influence the structure of the LLCs. More information about the microstructure of the LLCs phases are obtained by small angle X-ray scattering (SAXS, see Fig. ESI-1, ESI†). For better reproducibility, all samples were equilibrated in air after being dried from aqueous solution. All samples show a distinct SAXS pattern containing 1–3 signals. With increasing length of the hydrocarbon chain the surfactant size increases. A shift of the LLC lattice planes to larger distances and, according to Braggs law, a shift of the diffraction signals to lower scattering vectors q would be expected. This is exactly what we can extract as qualitative result from Fig. 3d and e.

For the saturated surfactants the lattice distance corresponding to the most intensive signal (d_{max}) linearly depends on the length of the hydrocarbon chain. Comparing a surfactant containing an unsaturated tail with the saturated counterpart, it is seen that the d_{max} value for **ManαC$_{12}$** is 0.2 nm smaller than d_{max}(**ManαC$^{uns}_{12}$**) = 2.7 nm. This effect can be explained by the influence of the C=C bond, which hampers an ordered arrangement of the carbohydrate chain and leads to an increased lattice spacing. Furthermore, the latter value corresponds well to the double of the molecular length of **ManαC$^{uns}_{12}$**. A distance resembling twice the molecular length is expected for almost any LLC-phase. In comparison, the **ManβC$_n$** compounds exhibit d_{max} values, which are approx. 0.2 nm larger, which can be attributed to the more linear arrangement of head group and tail of the β-linked surfactants. The head group has an influence as well, and it seems that the LLC phases of galactosides are slightly larger than for the mannosides. In combination, one can shift d_{max}(**ManαC$_{12}$**) = 2.5 nm to d_{max}(**ManβC$^{uns}_{12}$**) = 3.3 nm (Fig. 3e), although P is almost constant for these two surfactants.

The precise assignment of a supramolecular structure is difficult, if only a limited number of diffraction signals is available as in the current case, and one cannot exclude that mixtures of different phases occur. However, a satisfactory agreement was found to the pattern created by a so-called ordered bicontinuous double diamond phase (OBDD, space group *Pn3m*) with a lattice constant of a = 3.831 nm for **ManαC$_{10}$** as shown in Fig. 3d. The OBDD structure itself has been found rarely in general,[37,38] and to the best of our knowledge it has not been reported for a carbohydrate-based surfactant. OBDD is a complex structure formed by the interpenetration of two diamondoid networks. It is interesting to note that researchers recently have discussed the correlation between such structures and chirality.[39]

3.3.2 Aggregate formation in water at low concentration. There are several parameters of interest for the characterization of surfactants. Information about intermolecular interactions can be obtained from thermodynamic data (ΔG_{ag}, ΔH_{ag}, ΔS_{ag}). The concentration at which a surfactant forms aggregates in aqueous solution (≅CAC) and the size of these aggregates (D_{ag}) also provides important information. Prior to aggregate formation, the water–air interface gets occupied by the surfactants. The packing of the surfactants is expected to influence the minimum surface tension (γ_{min}) and the minimum molecular area occupied at the interface (A_{min}). For the determination of the mentioned features, we applied a combination of analytical techniques including isothermal titration calorimetry (ITC), concentration-dependent surface tension measurements and dynamic light scattering (DLS).

Fig. 4a exemplarily shows the integrated ITC curve for one measurement of the novel unsaturated surfactant **GalβC$^{uns}_{12}$**.

Each ITC measurement was repeated several times yielding consistent data. The ITC curves of other surfactants involved in the current study are given in Fig. ESI-2 (ESI†). For **GalβC$^{uns}_{12}$**, an aggregation point at a concentration of c = 1.12 ± 0.08 mM becomes visible, which corresponds to the CAC of this surfactant. In an ITC experiment, concentrated solutions of surfactants were titrated into water. With this technique, the heat that is produced during titration is detected. From this, thermodynamic values for the de-aggregation process upon dilution can be directly derived. Assuming reversible processes, which is typically the case for soft-matter interactions, the thermodynamic functions for aggregation and de-aggregation are equitable, but with opposite sign. For **GalβC$^{uns}_{12}$** we obtained ΔG_{ag} = −26.35 kJ mol^{-1} and ΔH_{ag} = 2.40 kJ mol^{-1}.

Concentration-dependent surface tension (γ) was also used as additional technique to determine the CAC (see Fig. 4b for **GalβC$^{uns}_{12}$** and Fig. ESI-3, ESI† for the other surfactants samples). The γ–c curve of **GalβC$^{uns}_{12}$** exhibits features, which are characteristic for surfactants. With increasing concentration, more and more molecules get located at the water–air interface. Consequently, γ decreases until the interface is fully occupied. At this point aggregation in solution takes place, and the slope of the γ–c changes. The CAC was determined as 1.05 mM from the tensiometry data (Fig. 4b), which is in good agreement with the ITC measurements. The value for surface tension reached at this transition (γ_{min}) is 28.3 mN m^{-1}, which is at the lowest end for surfactants with alkyl side chains and non-ionic head groups.[40,41]

From DLS measurements at three different concentrations, we obtained particle size distribution curves which are shown in Fig. 5a. Below the CAC, as expected, the scattering intensity is very low and there are barely any aggregates observable. At c = CAC, significant scattering, originating from objects 25 nm in diameter, can be observed. Upon raising the concentration the aggregate size increases (D_h = 60 nm). The latter findings can be confirmed by transmission electron microscopy under cryogenic conditions taken from **GalβC$^{uns}_{12}$** dispersions at c = CAC and 3 × CAC (Fig. 5c and d). At c = CAC a large number of particles with a diameter of ≈25–30 nm is visible. The size of the particles (100–300 nm) has increased significantly at c = 3 × CAC. The dimension of a conventional, spherical micelle would be of the order of 2-times the diameter of the surfactant (2 × 1.8 nm ≈ 3.6 nm). The observed aggregates are obviously much larger. It has been reported in the literature,[42] that sugar-based surfactants have a high tendency for the formation of non-equilibrium aggregates in water.

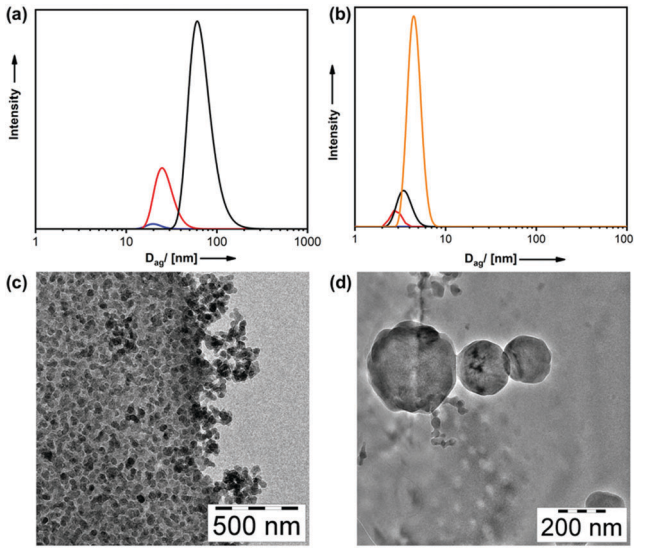

Fig. 5 (a) DLS data of **GalβC$^{uns}_{12}$** in water at c = 0.5 × CAC (blue), c = CAC (red) and c = 2 × CAC (black). (b) DLS data of **GalβC$_8$** in water at c = 0.1 × CAC (blue), c = CAC (red), c = 2 × CAC (black) and c = 5 × CAC (orange). Cryo-TEM micrographs of **GalβC$^{uns}_{12}$** at c ≈ CAC (c) and c ≈ 3 × CAC (d).

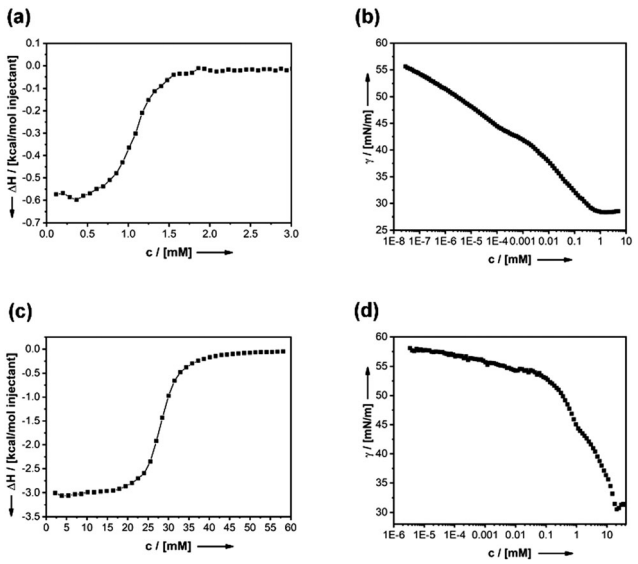

Fig. 4 (a) Integrated ITC curve and (b) tensiometry curve of **GalβC$^{uns}_{12}$** in water. (c) Integrated ITC curve and (d) tensiometry curve of **GalβC$_8$** in water.

The same set of data was acquired for all other compounds of the series shown in Fig. 1 (refer to the ESI†). As example with a shorter chain, the data for surfactant **GalβC$_8$** is shown in Fig. 4c, d and 5b. Because the length of the hydrocarbon chain affects the packing parameter and the HLB value, a significant change of the surfactant parameters is expected for **GalβC$_8$**, and this is exactly what we found. DLS measurements revealed small aggregate sizes of 4.4 nm only slightly rising at higher concentrations, which suggests the presence of micelles. In addition, ITC and tensiometry data are in agreement. We could confirm that the used methods resulted in reliable data about the surfactants' behavior, giving the possibility to analyze the data for systematic correlations.

The dependencies on the hydrocarbon chain length is the most obvious correlation, as indicated in the last paragraph. The most influenced factor is the CAC as seen from Fig. 6a. For aggregate formation of glycoside surfactants with C_n = 6, high concentrations (>100 mM) are required. Doubling of the chain length (C_n = 12) leads to a decrease of CAC by two orders of magnitude. This effect found for our carbohydrate surfactants

is stronger compared to classical ionic surfactants such as sodium alkyl sulfates (*e.g.* sodium dodecyl sulphate, SDS), where an increase of only one order of magnitude comparing C_6 with C_{12} tailed surfactants is found.[43,44] Because the monosaccharide-surfactants with longer alkyl chains showed reduced solubility in water, it was not possible to determine the CAC for a chain-length >8 and >10, respectively.[42] However, the solubility increased for the novel surfactants containing the unsaturated C_{12} carbon chain. We found that their CAC values lie above the line for the extrapolation to $n = 12$ of the respective saturated compounds. Again, as for the lyotropic liquid crystals described before, the presence of the C=C double bond has a remarkable effect. This may arise from an unfavorable conformation of the hydrocarbon chain, which is beneficial for a better solubility.

For the thermodynamic data, some distinct trends can be identified. The free enthalpy of aggregation ΔG_{ag} depends almost linearly on C_n (Fig. 6b). Considering the ΔH_{ag} values, which are slightly positive, it was found that the aggregation of the surfactants in water is predominantly entropy-driven. This effect was assigned in surfactant chemistry to the so-called hydrophobic effect.[45] Because water molecules cannot solvate the hydrophobic chain of the surfactant, they have to adopt an entropically unfavorable state for a single surfactant molecule in solution. When aggregates like micelles form, these water molecules are released gaining entropy. Thus, it is expected that the influence of entropy increases with longer alkyl chains, which is also in agreement with our data. The decrease of ΔH_{ag} with increasing C_n indicates, that the overall interaction becomes less repulsive, which can be explained by the increasing van der Waals interaction between the extended hydrocarbon chains. Comparing surfactants of the same chain length (*e.g.* C_8) but with different head groups reveals that the ΔH_{ag} values differ from each other, which is a sign for the strong influence of different head groups.

Regarding the aggregate size, a general trend exists as well. Here, on can distinguish between the cases, where micellar aggregates are formed, and those with formation of larger aggregates (Fig. 6c). Because the diameter of a spherical micelle equals in good approximation twice the length of a surfactant, the observed increase with longer hydrophobic chain is expected. The size of aggregates, which are much larger than micelles, qualitatively increases with longer alkyl chains as well. The transition from micelles to larger aggregates is influenced by the head group. Maltoside surfactants remain in the micellar state even for a long alkyl chain such as C_{12}. In the case of galactoside- or mannoside surfactants, the transition occurs already for C_8 and C_{10} chains, respectively, as indicated by the dashed lines in Fig. 6c. It can also be seen, that the anomeric configuration has a strong impact. For the galactose- as well as the glucose-based surfactants there is a remarkable difference in aggregate size for the α-form compared to the β-form indicated by the arrows in Fig. 6c.

The influence of the head group can be evaluated in further depth by taking a closer look at the tensiometry data. By calculating the maximum surface excess concentration Γ_{exc}, the minimum molecular area of the surfactant occupied at the air–water interface A_{min} can be determined. Although the molecular mass of the head group is the same or very similar

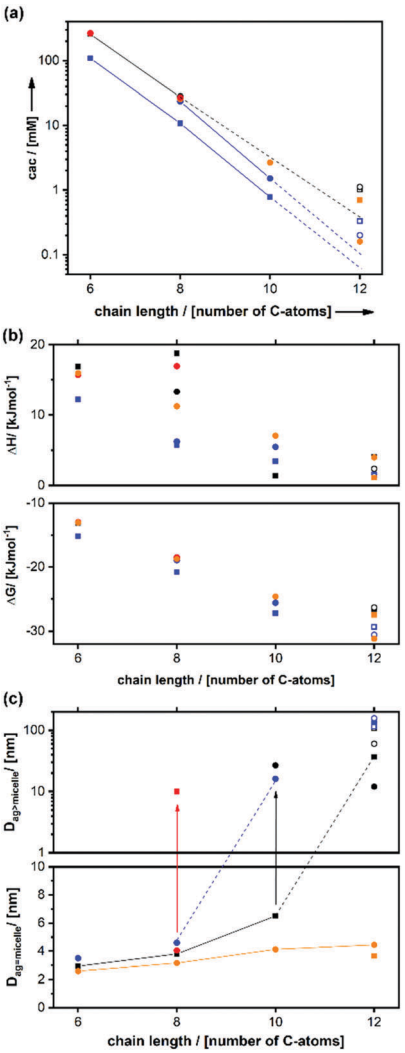

Fig. 6 (a) CAC–C_n correlation (dashed lines represent linear extrapolation). (b) ΔG_{ag} (circles) and ΔH_{ag} (squares)–C_n correlation. (c) Size of aggregates–C_n correlation at $c = 2 \times$ CAC; dashed lines = transition micellar to larger aggregates, arrows = difference between anomers, Gal (black), Man (blue), Glc (red), Mal (orange), α (squares), β (circles), C_n (solid symbols), $C^{uns}{}_n$ (hollow symbols).

(in the case of xylose) in the cases presented in Fig. 7, the mannoside head groups occupy a significantly higher surface area than the xyloside head groups. It can be understood that the surface tension reached at $c >$ CAC (γ_{min}) is smaller for smaller values of A_{min}, because the alkyl chains can pack denser at the air–water interface.

The anomeric conformation should also influence the way the surfactants pack at the air–water interface (see also Fig. 1). Therefore, it is not surprising that α- and β-forms differ, if all other parameters are kept constant. This effect can arise from the "molecular kink" introduced in the α-form, which leads to an increase in A_{min}. However, it is not expected that the alkyl chains pack denser as indicated by the lower γ_{min} values.

3.3.3 Emulsification properties. Another important application of surfactants is their use as emulsifiers. According to their HLB values (10.3–16.0; see Fig. ESI-4, ESI†) the surfactants

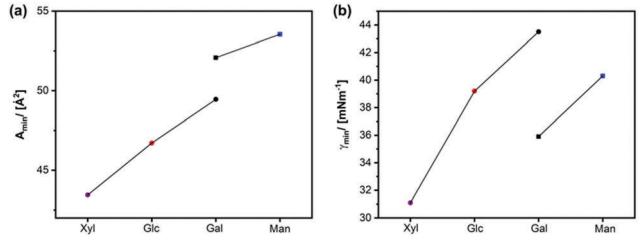

Fig. 7 Head group dependency of the minimum area occupied at the air–water interface (a) and the minimum surface tension at saturation at the interface (b). C_{12}-Surfactants: Xyl (purple), Gal (black), Man (blue), Glc (red), α (squares), β (circles).

from our library should be suitable for preparing oil-in-water (O/W) emulsions. Therefore, as test system, we emulsified cyclohexane in water (for a detailed procedure see the Experimental section). The stability of the emulsion was monitored over time by recording the volume of the phases formed by potential demixing (see Fig. 8a). Photographic images of a representative series are shown in Fig. 8b. As reference compounds, we used two commercially available emulsifiers: sorbitane monolaureate (Span 20) and octylphenol ethoxylate (Triton-X 100). After emulsification, demixing starts very slowly

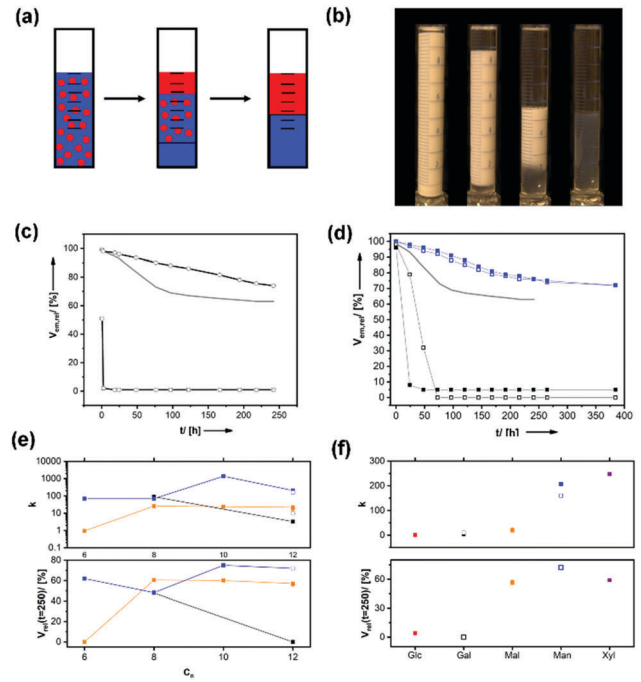

Fig. 8 (a) Graphic representation of the method used for determining the temporal stability of the formed emulsions. (b) Photographic images of an emulsion experiment with **GalαC$^{uns}_{12}$** at t = 0, 24, 48 and 72 h. (c) Remaining, relative emulsion volume *versus* time curve for three selected examples; grey line = reference span 20; circles = **ManαC$_{10}$**; squares = **MalβC$_6$**. (d) Comparison of relative emulsion volume *versus* time of emulsions stabilized by saturated and novel surfactants. (e) Emulsion stability parameters depending on hydrocarbon chain length. (f) Emulsion stability parameters depending on head group. Gal (black), Man (blue), Glc (red), Mal (orange), Xyl (purple), α (squares), β (circles), C_n (solid symbols), $C^{uns}{}_n$ (hollow symbols).

for Span 20, and, after 250 h, still 63% of the entire volume remains as emulsion (Fig. 8c). The short-chain maltoside **MalβC$_6$** turned out to be not suitable as emulsifier at all. Within minutes, the entire emulsion was separated. With increasing alkyl chain length (C_{10}), the surfactants stabilize the emulsion even better than Span 20.

Fig. 8d shows the emulsification behavior of the novel surfactants **ManαC$^{uns}_{12}$** and **GalαC$^{uns}_{12}$** in comparison to their saturated counterpart. It is noticeable that the saturated and unsaturated surfactants of the same head group exhibit nearly identical stabilization capabilities. This suggests that the unsaturated surfactants are promising substitutes (higher solubility, but similar emulsification behavior) for the saturated surfactants. However, it is obvious that the choice of headgroup greatly impacts the performance of the surfactant (see also Fig. 8f). For better comparison, we seek to parameterize the time dependent curves.

One parameter obviously is the remaining volume of the emulsion at t = 250 h. The demixing process was fitted by a mono-exponential decay ($V_{em,rel} \propto \exp(-t/k)$), and k was used as parameter for the description of the emulsions stability as well. Thus, high k values characterize a stable emulsion, which demixes slowly. Fig. 8e shows the two described parameters for a series of surfactants differing in hydrocarbon chain length C_n. Please note the logarithmic scale of the y-axis, indicating there are huge differences in how fast the emulsions destabilize. There is no uniform trend, however, a chain length of $n > 8$ seems to be beneficial for the performance as emulsifier, which is reasonable, because the HLB value decreases in this direction. In contrast to the properties discussed before, there are only minor differences observed regarding a change in the anomeric configuration or regarding the presence of an unsaturated side chain. The overall best emulsifiers from our library were found to be **ManαC$_{10}$**, **ManαC$_{12}$** and **ManαC$^{uns}_{12}$**, which exhibited nearly identical emulsifier properties. Surfactants with the same C_n have the same HLB value and should, thus, also perform equally as emulsifiers. This statement is wrong as seen from Fig. 8f for n = 12. Here, the head group has a huge influence on the stability of the emulsion. However, giving a universal explanation for these differences proves difficult, as many factors have to be taken into account for such complex, ternary systems (ratio of surfactant, water and hydrocarbon, polarity of the latter). However, from our experiments, we can deduce, that the rather small differences between our surfactants, introduced by change of the anomeric configuration and/or epimerisation of distinct OH-moieties in the carbohydrate headgroup, can impact their performance to the same degree as changing the size/polarity of the headgroup or changing the length of the hydrophobic moiety.

3.3.4 Glycoside surfactants as capping agents. Emulsions can be used in very different ways. One very special applications is in microemulsion-based techniques for the generation of inorganic particles.[46,47] In the past we have described a method for the preparation of ZnO nanoparticles by a microemulsion-based technique.[20–23] In our approach, a water in oil emulsion is prepared and an oil-soluble, organometallic ZnO precursor is

added. Although based on the HLB concept (see above) our surfactants are expected to be more suitable for (O/W) emulsions, it is important to note not only the temperature is higher (T = 55 °C), which could lead to a change in the behavior of the surfactant,[48] but we also work under steady shearing force resp. continuous application of ultrasound. This precursor reacts in a defined way with water, resulting in crystalline ZnO.[49] The emulsifying agent can interact with different facets of the growing ZnO nanoparticle by stabilizing them.[20,23,50] If certain facets can be selectively stabilized, this will influence the morphology of the particle.[51] Because of the demonstrated variability of the head group of carbohydrate-based surfactants, it could be, thus, highly interesting to investigate their behavior as capping agents. Up to this point, we could show that the surfactants can be used to form emulsions. Although it is beyond the scope of this paper to report about the ZnO nanoparticle synthesis in a comprehensive way, we demonstrate as proof-of-concept, that the glycoside-surfactants of this study are suitable for the generation of ZnO nanoparticles. With these experiments, we wanted to answer the question if there is a morphological effect or not. Therefore, the experiment depicted in Fig. 9a was performed.

Water in cyclohexane emulsions were prepared with either **MalβC$_{12}$** or **GalαC$_{12}$**. The ZnO precursor was then added (for detailed procedure refer to the experimental part). From the reaction, a white dispersion is obtained. After removal of solvent, powder X-ray diffraction (PXRD) was conducted. The resulting patterns (Fig. 9b) clearly show that in both cases ZnO with Wurtzite structure was obtained. Other crystalline phases are not present, and there are no marked differences by comparing the samples prepared using the two surfactants.

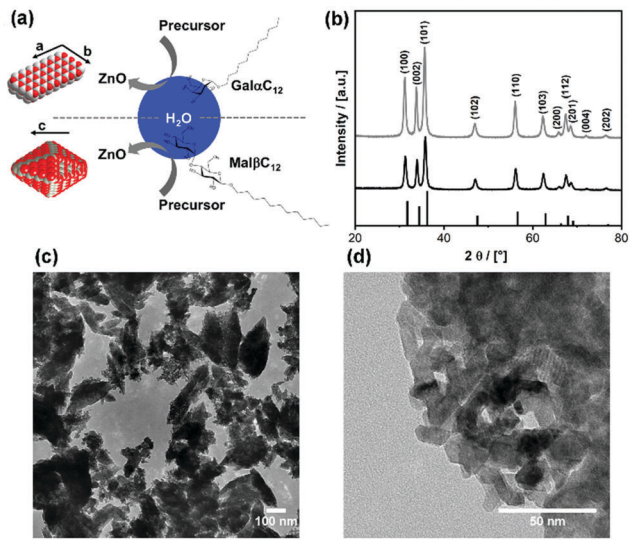

Fig. 9 (a) Schematic representation of the emulsion-based method for ZnO nanoparticle synthesis using carbohydrate-based surfactants. Two resulting particle morphologies are shown (grey = Zn; red = O). (b) PXRD patterns of the ZnO materials resulting from **MalβC$_{12}$** (grey) and **GalαC$_{12}$** (black) in comparison to the reference pattern of crystalline ZnO in Wurtzite structure (black bars). TEM micrographs of ZnO particles obtained using **MalβC$_{12}$** (c) and **GalαC$_{12}$** (d).

Transmission electron microscopy (TEM) measurements show that the samples are morphologically different as shown in Fig. 9c, d and Fig. ESI-5 (ESI†). The use of **MalβC$_{12}$** led to the formation of particles with a shape resembling a rugby ball. As interesting as this shape may seem, it actually represents nanoparticles in the so-called Wulff form. The Wulff form is the shape a crystal adopts solely on the intrinsic stability of its facets.[51] Therefore, it can be concluded, that the energy of surfaces terminating the crystal was not influenced by **MalβC$_{12}$** during growth. This result indicates that the maltose head group does not specifically interact with the ZnO crystal. The ZnO particle shape found for **GalαC$_{12}$** is much different from the Wulff form. The particles have a rhombus-like shape with the edges forming angles of 120° and 60°, respectively (see Fig. ESI-5, ESI†). Therefore, we assume the shape proposed in Fig. 9a. This is in agreement with the good fit of the measured atomic plane distance (2.8 Å) to the literature value for the (100) plane (2.81 Å). In addition to a restriction of growth in crystallographic *c*-direction, **GalαC$_{12}$** seems to stabilize the (100) and the (010) facets. Particles with crystallographic *a*,*b*-direction as main directions of growth are not unusual.[52,53] However, these particles do typically represent hexagonal plates or variants of it. The more rod-like morphology in combination to this particular crystallographic orientation is unusual to the best of our knowledge. Based on these first promising findings we will further investigate the potential of our surfactant library for nanoparticle synthesis.

4 Conclusions

In this work, we presented a library of well-defined glycosurfactants. Besides known, saturated alkyl-glycosides, we could successfully introduce a novel class of glycosurfactants bearing an internally unsaturated alkyl chain. From our library's compounds, we could investigate the influence of alkyl chain length/structure, carbohydrate moiety and anomeric configuration on the properties of the surfactants. From our data, we can conclude that the chain length influences the parameters of the surfactants (d_H, CAC, thermodynamic parameters) as expected. The novel unsaturated surfactants show a differing behavior, which arises from a bent shape of the alkyl chains. We could also find significant differences for changes in the head group. The sugar moiety as well as the anomeric configuration led to different CACs and also greatly impacted the emulsification capabilities of the surfactants. The most important take-home message of our study is, although invariant in packing parameter and HLB value, surfactant isomers do vary significantly in almost all key properties.

Two promising surfactants were then, as proof-of-principle, tested as capping agents for the generation of anisotropic ZnO nanocrystals. We could show that subtle changes in the carbohydrate head group can indeed induce changes in nanoparticle growth. With these findings, we will now further explore the potential of glycosurfactants for the synthesis of defined, anisotropic nanoparticles.

Conflicts of interest

There are no conflicts to declare.

Acknowledgements

The project was supported by the Deutsche Forschungsgemeinschaft (collaborative research center SFB 1214, project A1). R. M. M. acknowledges a PhD fellowship from the Konstanz Research School Chemical Biology. M. K. was funded by an ERC consolidator grant (ISURF, project 614606). We thank A. Friemel and U. Haunz for their assistance with NMR spectroscopy and M. Krumova for Cryo-TEM support.

Notes and references

1 *Non-Ionic Surfactants*, ed. P. L. Wendt and D. Hoysted, Nova Science Publishers, Inc., 2010.
2 L. J. Chen, S. Y. Lin, C. C. Huang and E. M. Chen, *Colloids Surf., A*, 1998, **135**, 175–181.
3 J. Eastoe and J. S. Dalton, *Adv. Colloid Interface Sci.*, 2000, **85**, 103–144.
4 P. K. Vemula and G. John, *Acc. Chem. Res.*, 2008, **41**, 769–782.
5 J. D. Desai and I. M. Banat, *Microbiol. Mol. Biol. Rev.*, 1997, **61**, 47–64.
6 E. Fischer and B. Helferich, *Justus Liebigs Ann. Chem.*, 1911, **383**, 68–91.
7 W. von Rybinski and K. Hill, *Angew. Chem., Int. Ed.*, 1998, **37**, 1328–1345.
8 D. Blunk, P. Bierganns, N. Bongartz, R. Tessendorf and C. Stubenrauch, *New J. Chem.*, 2006, **30**, 1705–1717.
9 H. Abdelkader, A. W. G. Alani and R. G. Alany, *Drug Delivery*, 2014, **21**, 87–100.
10 R. Rajera, K. Nagpal, S. K. Singh and D. N. Mishra, *Biol. Pharm. Bull.*, 2011, **34**, 945–953.
11 M. Beller, J. G. E. Krauter, A. Zapf and S. Bogdanovic, *Catal. Today*, 1999, **48**, 279–290.
12 M. Hager and K. Holmberg, *Tetrahedron Lett.*, 2000, **41**, 1245–1248.
13 Y. Y. Luk and N. L. Abbott, *Curr. Opin. Colloid Interface Sci.*, 2002, **7**, 267–275.
14 J. N. Israelachvili, D. J. Mitchell and B. W. Ninham, *J. Chem. Soc., Faraday Trans. 2*, 1976, **72**, 1525–1568.
15 W. C. Griffin, *J. Soc. Cosmet. Chem.*, 1954, **5**, 249–256.
16 V. Vill, T. Bocker, J. Thiem and F. Fischer, *Liq. Cryst.*, 1989, **6**, 349–356.
17 P. Sakya, J. M. Seddon and V. Vill, *Liq. Cryst.*, 1997, **23**, 409–424.
18 V. Vill and R. Hashim, *Curr. Opin. Colloid Interface Sci.*, 2002, **7**, 395–409.
19 J. Schmidt-Lassen and T. K. Lindhorst, *MedChemComm*, 2014, **5**, 1218–1226.
20 C. Lizandara-Pueyo, S. Siroky, M. R. Wagner, A. Hoffmann, J. S. Reparaz, M. Lehmann and S. Polarz, *Adv. Funct. Mater.*, 2011, **21**, 295–304.
21 C. Lizandara-Pueyo, S. Dilger, M. R. Wagner, M. Gerigk, A. Hoffmann and S. Polarz, *CrystEngComm*, 2014, **16**, 1525–1531.
22 M. Gerigk, P. Ehrenreich, M. R. Wagner, I. Wimmer, J. S. Reparaz, C. M. S. Torres, L. Schmidt-Mende and S. Polarz, *Nanoscale*, 2015, **7**, 16969–16982.
23 M. Gerigk, J. Bahner, T. Kollek, S. Helfrich, R. Rosenberg, H. Cölfen and S. Polarz, *Part. Part. Syst. Charact.*, 2017, **34**, 1600215.
24 W. Klotz and R. R. Schmidt, *J. Carbohydr. Chem.*, 1994, **13**, 1093–1101.
25 T. Ren and D. Liu, *Tetrahedron Lett.*, 1999, **40**, 7621–7625.
26 J. Zhang and P. Kováč, *J. Carbohydr. Chem.*, 1999, **18**, 461–469.
27 G. Zemplén and E. Pacsu, *Ber. Dtsch. Chem. Ges.*, 1929, **62**, 1613–1614.
28 Y. Du, M. Zhang, F. Yang and G. Gu, *J. Chem. Soc., Perkin Trans. 1*, 2001, 3122–3127.
29 J. Ohlsson and G. Magnusson, *Carbohydr. Res.*, 2000, **329**, 49–55.
30 R. Lopez and A. Fernandez-Mayoralas, *J. Org. Chem.*, 1994, **59**, 737–745.
31 M. Horiike and C. Hirano, *Agric. Biol. Chem.*, 1980, **44**, 2229–2230.
32 J. M. Chong, M. A. Heuft and P. Rabbat, *J. Org. Chem.*, 2000, **65**, 5837–5838.
33 S. Paula, W. Sues, J. Tuchtenhagen and A. Blume, *J. Phys. Chem.*, 1995, **99**, 11742–11751.
34 G. Chen, Z. Li, L. Chen, S. Ji and W. Shen, *J. Dispersion Sci. Technol.*, 2017, **38**, 506–514.
35 K. Bock and C. Pedersen, *J. Chem. Soc., Perkin Trans. 2*, 1974, 293–297.
36 G. Milkereit, V. M. Garamus, K. Veermans, R. Willumeit and V. Vill, *J. Colloid Interface Sci.*, 2005, **284**, 704–713.
37 E. L. Thomas, D. B. Alward, D. J. Kinning, D. C. Martin, D. L. Handlin and L. J. Fetters, *Macromolecules*, 1986, **19**, 2197–2202.
38 C. Y. Chu, X. Jiang, H. Jinnai, R. Y. Pei, W. F. Lin, J. C. Tsai and H. L. Chen, *Soft Matter*, 2015, **11**, 1871–1876.
39 C. Dressel, F. Liu, M. Prehm, X. B. Zeng, G. Ungar and C. Tschierske, *Angew. Chem., Int. Ed.*, 2014, **53**, 13115–13120.
40 N. M. Kovalchuk, A. Trybala, V. Starov, O. Matar and N. Ivanova, *Adv. Colloid Interface Sci.*, 2014, **210**, 65–71.
41 W. H. Ansari, N. Fatma, M. Panda and D. Kabir-ud, *Soft Matter*, 2013, **9**, 1478–1487.
42 H. L. Lu, I. Pezron, T. Gaudin and A. Drelich, *Colloids Surf., A*, 2018, **540**, 10.
43 A. M. Tedeschi, E. Busi, L. Paduano, R. Basosi and G. D'Errico, *Phys. Chem. Chem. Phys.*, 2003, **5**, 5077–5083.
44 F. A. Alejandra and B. D. Carlos, *Helv. Chim. Acta*, 2007, **90**, 1141–1151.
45 P. Alexandridis, J. F. Holzwarth and T. A. Hatton, *Macromolecules*, 1994, **27**, 2414–2425.
46 M. A. Malik, M. Y. Wani and M. A. Hashim, *Arabian J. Chem.*, 2012, **5**, 397–417.
47 A. K. Ganguli, A. Ganguly and S. Vaidya, *Chem. Soc. Rev.*, 2010, **39**, 474–485.

48 S. de Oliveira Honse, K. Kashefi, R. M. Charin, F. W. Tavares, J. C. Pinto and M. Nele, *Colloids Surf., A*, 2018, **538**, 565–573.
49 C. Lizandara-Pueyo, M. W. E. van den Berg, A. De Toni, T. Goes and S. Polarz, *J. Am. Chem. Soc.*, 2008, **130**, 16601–16610.
50 C. Lizandara-Pueyo, M. C. Morant-Minana, M. Wessig, M. Krumm, S. Mecking and S. Polarz, *RSC Adv.*, 2012, **2**, 5298–5306.
51 S. Polarz, *Adv. Funct. Mater.*, 2011, **21**, 3214–3230.
52 Z. R. R. Tian, J. A. Voigt, J. Liu, B. McKenzie, M. J. McDermott, M. A. Rodriguez, H. Konishi and H. F. Xu, *Nat. Mater.*, 2003, **2**, 821–826.
53 C. H. Ye, Y. Bando, G. Z. Shen and D. Golberg, *J. Phys. Chem. B*, 2006, **110**, 15146–15151.